Interannual Variability in Global, Upper-Ocean Heat Content, Temperature and Thermosteric Sea-Level Rise

Josh Willis, Dean Roemmich, Bruce Cornuelle
jkwillis@ucsd.edu, droemmich@ucsd.edu, bcornuelle@ucsd.edu,
Scripps Institution of Oceanography

Introduction

Because of its large heat capacity and organized circulations, the ocean plays important roles in the Earth's climate system through the storage and transport of heat. As globally averaged atmospheric temperature rises, it becomes increasingly important to quantify the ocean's ability to absorb and sequester excess heat, as well as to understand how a heated ocean affects the atmosphere and cryosphere. Describing the variability of the ocean's thermal properties is therefore an important step toward understanding its role in the global heat budget. In the present study, we combine satellite altimetric height with *in situ* profiles to compute variability in global, upper-ocean heat content, temperature and thermosteric sea-level rise with unprecedented accuracy.

Data

For altimeter data, the AVISO merged, gridded product containing TOPEX/Poseidon and ERS 1 and 2 was used. This product provides sea surface height anomalies relative to a 7-year time-mean from 1993 to 1998. It consists of maps produced every 7 days on a 1/3˚ x 1/3˚ Mercator grid. Approximately 900,000 *in situ* profiles were collected from various databases from 1992-2002. Profiles include data from XBT, CTD, profiling floats, and moorings. A nine-year mean and a seasonal cycle were removed from both datasets prior to analysis. Heat content, Thermosteric expansion, and temperature were all calculated to 750m.

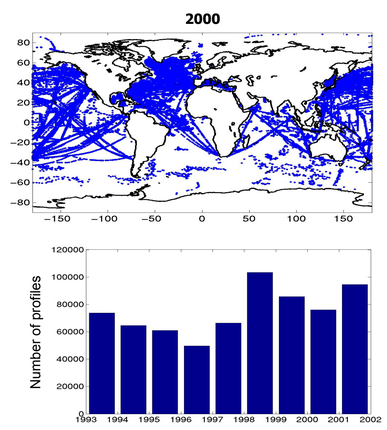

Figure 1. Time series of profile availability and profile distribution for the year 2000. Note the poor coverage in the southern hemisphere

The Difference Estimate

The estimates of heat content, temperature and thermosteric variability were calculated using the technique described by *Willis et al.* [2003] for combining satellite and *in situ* data. The technique, referred to here as the 'difference estimate,' relies on altimeter data to reduce errors caused by undersampling, but also directly includes *in situ* data to help improve the accuracy. Altimeter data is first combined with linear regression coefficients to produce an initial guess for the estimate. An objective map of the *in situ* data is then made relative to the initial guess. Thus, a variable derived from the *in situ* data, would be computed as follows:

$$< \mathrm{XBT} >_{\mathrm{estimate}} = < \mathrm{XBT} - \alpha\, \mathrm{AH} > + \alpha < \mathrm{AH} >, \qquad (1)$$

where XBT is the estimated quantity (e.g., heat content or thermosteric expansion), AH is altimetric height and α is the linear regression coefficient of AH onto XBT. The technique was developed and tested using high-resolution XBT (HRX) transects in the Tasman Sea region. Figure 2 shows the results from a subsampling experiment used to test the accuracy of the difference estimate against other estimates using various amounts of available *in situ* data. The experiment shows that regardless of the relative abundance of profile data, the difference estimate contains less error than estimates made using either profile data or satellite data alone.

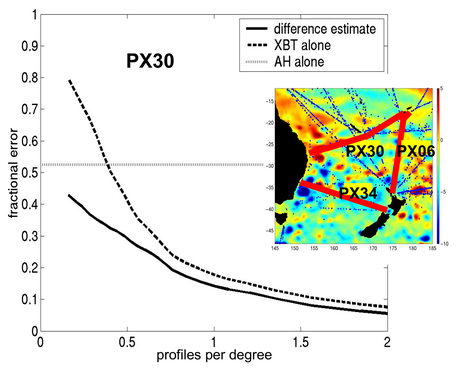

Figure 2. Fractional error in estimates of 0/800 m steric height along PX30 averaged over 36 repeats of the transect. Undersampling was simulated by leaving out profiles along the track when producing the estimates. The result was then compared with the "true" field which kept the full resolution of the transects. Note that the 'AH alone' estimate does not vary with sampling because the altimeter data were not subsampled. The three estimates shown are: Thick line—difference estimate. Dashed line—XBT data alone. Dotted line—altimetric height multiplied by a regression coefficient (note, this is the same as last term in equation 1). **Inset.** Tasman Sea Region. Red lines show WOCE HRX transects, background is altimetric height in cm.

Global Heat Content

Heat content is defined as the integral of $\rho C_p T(z)dz$ from the surface to 750 m. Maps of interannual variability in heat content were computed using the difference estimate. Figures 3 through 6 show various results obtained using the estimates of heat content and the associated heat storage (time derivative of heat content).

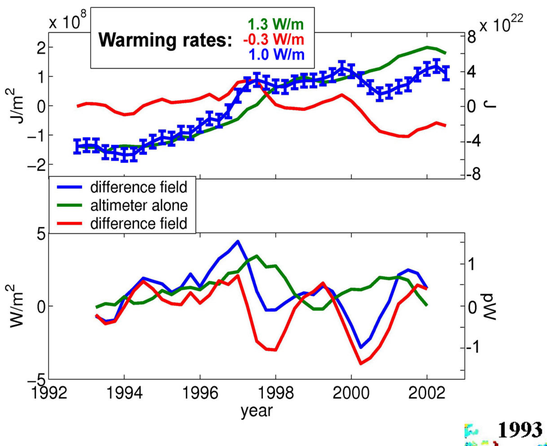

Figure 3. a). Global average heat content in J/m² (right scale shows integrated heat content in J). To illustrate the effect of including the *in situ* data directly, the regression estimate and difference field are also shown, these represent the second and first terms, respectively, of equation (1). Error bars are for the difference estimate are calculated using the altimeter data to estimate the effects of undersampling of the difference field by the *in situ* data. Average heating rates and their error bars are calculated from the 9-year differences of the curves. **b).** Same as **a)**, but for heat storage. Note that the difference field (which represents the contribution from the *in situ* data) contributes a substantial amount of interannual variability in both plots and also makes a significant contribution to the decadal warming rate in part **a).**

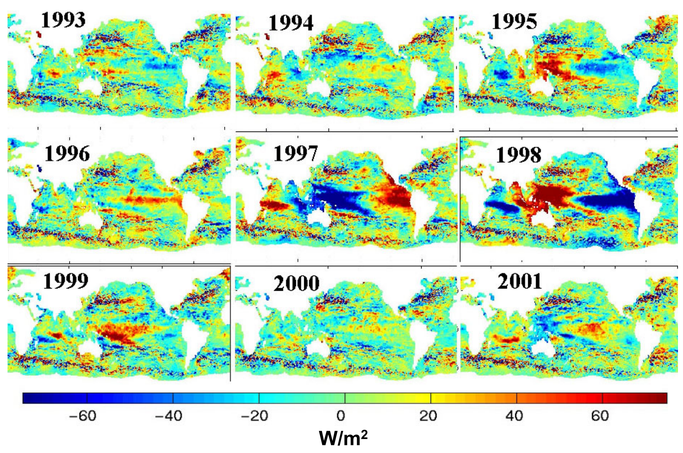

Figure 4. Maps of interannual heat storage variability. Note that the onset of the large 1997-98 El Nino event is represented by a cooling in the western tropical Pacific in 1997, followed by a subsequent warming of the same region in 1998 as the El Nino relaxed. Similar patterns of western tropical warming can be seen in 1995 marking the end of a persistent El Nino condition in the early 90's, and again in 1999 which marked the beginning of a protracted La Nina.

Heat Content (continued)

Heat content in the tropics is dominated by ENSO variability, the 1997-98 event resulted in a large oceanic uptake of heat in the tropics. Some of this heat appears to have propagated out of the tropics into mid-latitudes. Although the interannual variability is dominated by the tropics, the decadal trend in heat content is caused largely by the more steady warming at higher latitudes, particularly in the southern hemisphere.

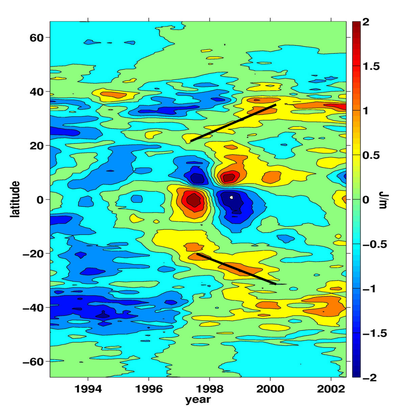

Figure 5. Zonal integral of heat content in Joules per meter of latitude. The integral, rather than the average was shown to reflect the contribution of each latitude band to the global average. The 1997-98 ENSO event is clearly visible in the tropics. Note the propagation of heat toward the poles illustrated by the thin lines. Note, also the steady warming in the southern hemisphere centered at 40˚ S.

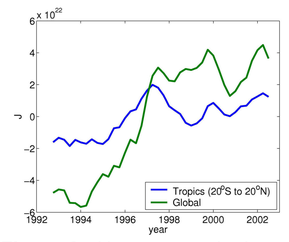

Figure 6. Heat content in the tropics and globally. Heat content in the tropics increased during the 1997-98 ENSO event, then fell off, being transported poleward into mid-latitudes.

Temperature

Maps of interannual variability in subsurface temperature were also computed using the difference estimate. Figures 7 and 8 show warming trends over the time series. These show that the strong warming pattern in the tropics associated with ENSO variability is confined largely to the surface layers, while warming in the southern hemisphere extends much deeper.

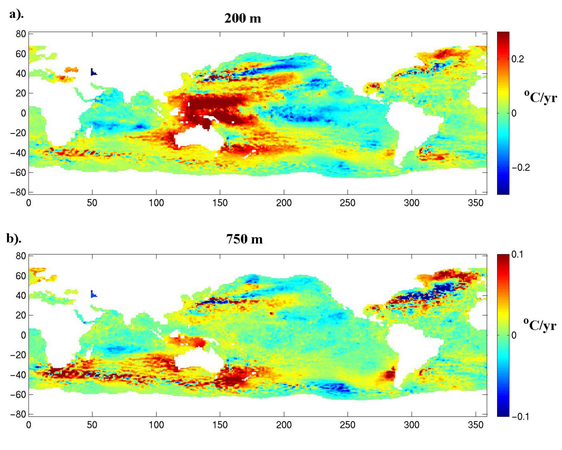

Figure 7. a). Temperature trend at 200 m and **b)** 750m. Note that the color scale in part **b)** is one third that of part **a).**

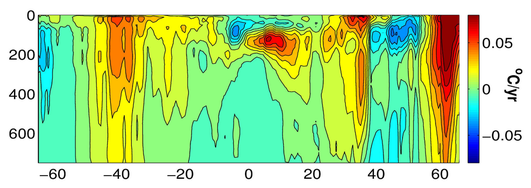

Figure 8. Warming trend as a function of depth and latitude. Note the relatively shallow warming in the tropics as compared to the southern hemisphere. Also, although the warming in the northern hemisphere is quite rapid, it contributes only slightly to the global trend because the latitude band centered at 60° N represent only a small fraction of the global ocean.

Thermosteric Sea-Level Rise

The difference estimate of thermosteric sea-level rise was calculated using the quantity:

$$\int_0^{750} \Delta T \cdot \gamma(S_C, T_C + \Delta T/2, P)dz$$

where γ is the thermal expansion coefficient, T_C and S_C are climatological temperature and salinity, and ΔT is the temperature anomaly relative to T_C. This quantity represents the local change in sea surface height due to thermal expansion and was calculated for each *in situ* profile before interannual maps were made using the difference estimate. Figure 9 shows the global mean thermosteric sea-level rise along with two recent estimates of total sea-level rise. The rate of thermosteric sea-level rise was 1.8 ± 0.3 mm/yr, estimated using the 9-year difference. Residuals suggest a eustatic sea-level rise of approximately 1.2 mm/yr.

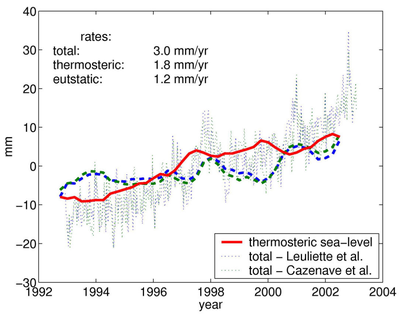

Figure 9. Mean sea-level rise in mm. The red curve shows thermosteric sea-level estimated in the present study. The dotted blue curve shows total sea-level as estimated by *Leuliette et al.* [in prep.]. The dotted green line is total sea-level as estimated by *Cazenave et al.* [pers. comm.]. Dashed lines show residuals.

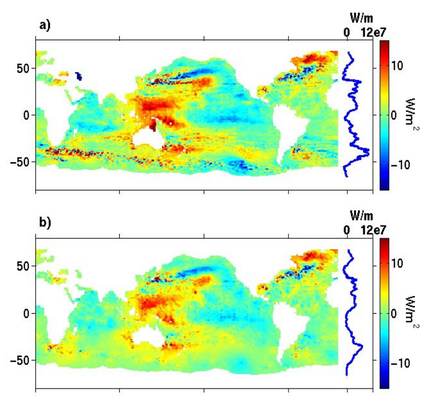

Figure 10. Maps of trend in heat content (in W/m²) and their zonal integrals (in Watts per meter of latitude). **a).** difference estimate. **b).** estimate made from maps using *in situ* data alone.

Summary and Conclusions

Using the technique described by *Willis et al.* [2003], satellite altimetric height and *in situ* data were combined to produce global, interannual estimates of heat content, temperature, and thermosteric sea-level variability. Globally averaged heat content shows strong interannual variability and has a warming rate of 1.0 ± 0.2 W/m² from 1993 to 2002 for the upper 750 m of the water column. As a result of the warming, thermosteric sea-level rises at a rate of 1.8 ± 0.3 mm/yr over the same time period. These results are fairly robust. To illustrate this, figure 10 shows maps of the heat content trend from the difference estimate along with a similar map made from *in situ* data alone. Clearly, most of the decadal warming signal can be recovered using *in situ* data alone, despite the scarcity of profiles. In the global average, the warming trend suggested by *in situ* data alone is 0.8 W/m²—within the error bars of the difference estimate. Furthermore, from figure 1, we expect the difference estimate to perform at least as well as (and probably better than) the *in situ* data alone. Tests have also shown the difference estimate to be fairly insensitive to large systematic changes in the intrinsic slope of the altimeter data.

References

Leuliette, E.W., R. S. Nerem, and G. T. Mitchum, Results of TOPEX/Poseidon and Jason-1 Calibration to Construct a Continuous Record of Mean Sea Level, *Marine Geodesy*, in preparation.

Willis, J. K., Roemmich, D., and B. Cornuelle, Combining altimetric height with broadscale profile data to estimate steric height, heat storage, subsurface temperature, and sea-surface temperature variability, *J. Geophys. Res.*, *108*, 3292, 2003.

Acknowledgements: Mean sea-level estimates were generously provided by Eric Leuliette at the University of Colorado, Boulder, and Anny Cazenave, Alix Lombard and Kien Do Minh at LEGOS-GRGS. The altimeter products were produced by the CLS Space Oceanography Division as part of the Environment and Climate EU ENACT project (EVK2-CT2001-00117) and with support from CNES. Combined analysis of TOPEX and XBT data is supported by NASA through the JASON-1 Science Working Team. The roles of all persons and agencies are gratefully acknowledged.